Coalescence dynamics of a droplet on a sessile droplet

Manish Kumar[a], Rajneesh Bhardwaj[a], Kirti Chandra Sahu[b,*]

[a]*Department of Mechanical Engineering, Indian Institute of Technology Bombay, Mumbai, 400076, India*
[b]*Department of Chemical Engineering, Indian Institute of Technology Hyderabad, Sangareddy 502 285, Telangana, India*

Abstract

The coalescence dynamics of an ethanol droplet freely falling on a sessile ethanol droplet is investigated experimentally using a high-speed imaging system. The regime maps showing the partial coalescence and spreading behaviors in the plane of the Weber number (*We*) and the volume of the sessile droplet (V_p) normalized with the volume of the impacting droplet (V_i) have been presented. The partial coalescence phenomenon is observed when the ratio of the volume of the sessile droplet to that of the impacting droplet (V_p/V_i) is greater than two. For $V_p/V_i = 2$, the size of the daughter droplet is found to be about 0.1 times as that the impacting droplet, which increases with the increase in the Weber number (*We*) and normalized volume of the sessile droplet. In the present study, the negative curvature of the droplet coupled with the presence of the substrate leads to a different coalescence dynamics.

1. Introduction

Coalescence of drops exhibits surprisingly complex dynamics that have been fascinating researchers for many decades [1, 2]. This phenomenon is observed in many engineering applications, such as viscous sintering, spray cooling, cloud formation, and also in the number of emerging micro- and nanofluidic technologies [3]. In many of these applications, drops either fall on a solid substrate or another liquid drop deposited earlier at the substrate. Thus several researchers have investigated the dynamics of drop impacting on solid surfaces (e.g. [4, 5]), collision of two spherical drops (e.g. [6]) and drop falling on liquid pool (e.g. [7]). In this context, below, we review the literature associated with the collision of the drop with another liquid-air interface.

A liquid drop freely falling on the free-surface of a liquid pool undergoes partial coalescence and spreading behaviors based on the associated physical parameters, such as the impacting velocity and the size of the drop, and also the fluid properties of the liquids. At low velocity, the drop floats on the free-surface while the trapped air between the drop and the free-surface drains out. Subsequently, a neck forms at the contact point of the drop and the free-surface that expands rapidly due to high capillary pressure. This generates capillary waves traveling in the upward direction and thus the interface expands, forming a liquid column. This is followed by squeezing of

*Corresponding author
Email address: ksahu@iith.ac.in (Kirti Chandra Sahu)

the column near the free surface due to surface tension, and a daughter drop pinches off from the liquid pool. Several researchers have found that the diameter of the daughter drop, d_s is about half of the impacting drop, d_i (e.g. see [8, 9]). The process gets repeated via a cascading process until the daughter drop completely drains in the liquid pool. This phenomenon is commonly termed as partial coalescence [7, 9]. Initially, it was believed that partial coalescence is a consequence of an inviscid instability [10], but later it was found that it is primarily governed by gravity, viscosity and interfacial tension ([8, 11]).

Although a large volume of previous investigations on this subject was dedicated to the dynamics of drops on horizontal liquid-air interface [11–17], very few studies focused on a drop impacting on another drop. Recently, Tang et al. [18] investigated the dynamics of drop impact on a thin liquid surface and studied the effect of the film thickness and the liquid viscosity on the bouncing and merging of the drop. They delineated the regimes associated with bouncing and merging in the Weber number and the film thickness space. Below, we highlight the studies of Zhang et al. [19], Graham et al. [20] and Deka et al. [6], which are most relevant to the present work as we investigate the partial coalescence dynamics of a drop freely falling on a sessile drop. However, there exist many studies (e.g., [21–26]) which have reported the coalescence and bouncing phenomena of two pendant spherical drops impacting with some velocities. In the case of horizontal air-liquid interfaces, few researchers have also investigated the effect of hydrophobic substrates on coalescence dynamics [27–29].

Zhang et al. [19] experimentally studied the behavior of drops (diameter in the range of 0.45 mm to 1.52 mm) falling on another drop resting on a steel nozzle. Water and glycerin/water mixtures were considered as the working fluids, such that the Bond number, $Bo = \rho g {d_i}^2/\sigma < 0.4$, where d_i is the diameter of the impacting drop, g is acceleration due to gravity, ρ is the density of the liquid and σ denotes the interfacial tension. They found that partial coalescence occurred when the ratio of the diameter of the drop resting on the nozzle to the diameter of the impacting drop was about 1.55, which increases with increasing the Ohnesorge number, $Oh = \mu/\sqrt{\rho\sigma d_i}$; μ being the dynamic viscosity of the liquid. Like in the case of a spherical drop freely falling on a liquid pool, the diameter of the daughter drop was found to be about half of that of the impacting drop. Graham et al. [20] studied the effect of wettability of solid substrate of the sessile drop on the coalescence behavior of an impacting drop by conducting experiments and numerical simulations. But the partial coalescence dynamics has not been reported in their study. Recently, Deka et al. [6] numerically studied the coalescence dynamics of two unequal sized spherical drops. They reported that the collision leads to partial coalescence of very small daughter drops even for diameter ratio 1.2. Here, it is also worth mentioning the study of Nikolopoulos et al. [30] who investigated coalescence dynamics of a droplet (4 mm diameter) on a sessile droplet, a configuration similar to the one considered in the present work. However, they focused on the splashing regime by impacting the droplet from a bigger height (150 to 440 mm). They studied the effect of the Weber (We) and Ohnesorge (Oh) numbers, and the contact angle of the sessile droplet on the crown and base diameter during splashing.

As the above literature review suggests, the coalescence dynamics of a drop impacting on a sessile drop leading to the partial coalescence phenomenon has not been studied yet, which is the focus of the present work. We experimentally investigate the dynamics of an ethanol drop freely falling under the action of gravity on a sessile ethanol drop using a high-speed camera. Unlike

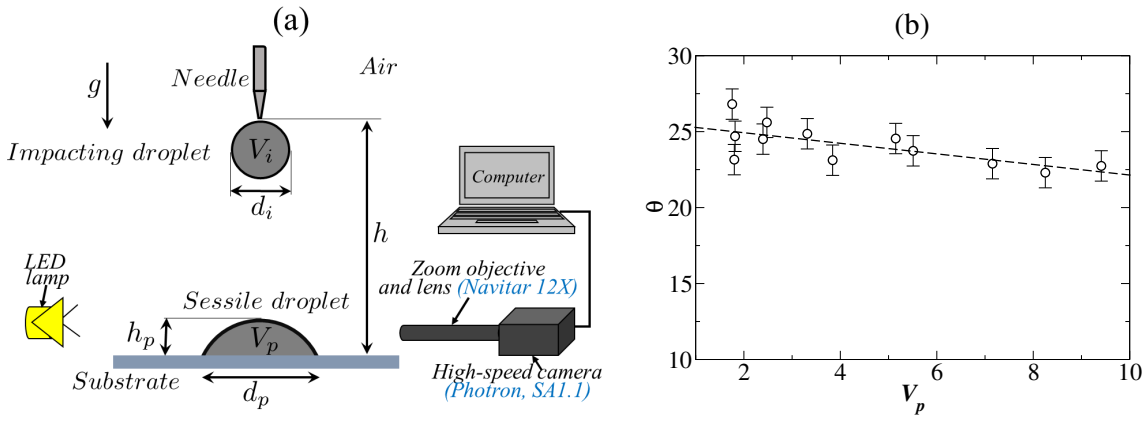

Figure 1: (a) Schematic diagram showing a freely falling ethanol droplet on a sessile ethanol droplet. The diameter and volume of the impacting and the sessile droplets are (d_i,V_i) and (d_p,V_p), respectively. The height of the needle from the substrate is h and the height of the sessile drop is h_p. (b) The variation of contact angle, θ (in degree) of the sessile droplet with its volume, V_p (in μl). The best fit line is $\theta = 25.61 - 0.347V_p$. The maximum error in contact angle measurement is $\pm 1^\circ$.

Nikolopoulos et al. [30], we consider low impacting height (2.4 to 5.9 mm) to refrain our study from splashing droplet impact regime and study the effect of the sizes of sessile and impacting droplets and impact height/velocity (the Weber number) on the partial coalescence dynamics. It is observed that the formation of daughter droplet occurs when $V_p/V_i \geq 2$, where V_p and V_i are the volume of the sessile and the impacting droplets, respectively. We found that the ratio of the volume of the daughter droplet (V_s) to that of the impacting droplet (V_i) is about 0.1 for $V_p/V_i = 2$, which increases as the height of the impacting droplet (or the Weber number (We)) and volume of the sessile droplet are increased. We observed that the reflected capillary waves from the contact angle and the curvature of the sessile drop play an important role in the coalescence dynamics.

The rest of the paper is organized as follows. The details of the experimental setup and procedure followed are given in Section 2. The results obtained from our study are presented in Section 3 and the concluding remarks are given in Section 4.

2. Experimental set-up

The main components of the experimental setup are glass substrates (Borosil Inc, India), a droplet injection mechanism that consists of commercially available needles and a syringe clamped in a retort stand, a high-speed camera (Photron Inc., SA1.1) along with back-lit illumination system and a computer. A schematic diagram of the experimental set-up is shown in Figure 1(a). A shadowgraphy technique has been used to visualise the sessile and impacting droplets. A LED lamp was used to improve the background. The high-speed camera, droplets and the LED lamp were positioned in-line to achieve high-quality shadowgraphy images. The entire set-up is kept on an optical table to make it perfectly level.

A spherical droplet of diameter d_i and volume V_i is freely falling on a sessile droplet of wetted diameter d_p and volume V_p resting on a glass substrate of dimensions 75 mm $\times$25 mm $\times$1 mm. The glass substrate is cleaned sequentially with deionized water and isopropanol and then it is dried

Table 1: The values of the Ohnesorge number ($Oh \equiv \mu/\sqrt{\rho\sigma d_i}$) and the Bond number ($Bo \equiv \rho g {d_i}^2/\sigma$) for different sizes of the impacting ethanol droplet. The value of the Atwood number, $At \equiv (\rho - \rho_a)/(\rho + \rho_a)$ is 0.997 for all the cases considered in the present study.

V_i (μL)	d_i (mm)	Oh	Bo
1.8	1.51	6.74×10^{-3}	0.799
2.5	1.70	6.36×10^{-3}	1.012
3.1	1.81	6.16×10^{-3}	1.147

using compressed ambient air. Because we used the glass substrate of the same brand and follow the same cleaning procedure, it can be assumed the roughness is the same for all glass substrates. The root mean square value of the roughness of glass slides is around 2.9 nm as reported in our previous work [31]. Different sizes of ethanol droplets are generated using commercially available needles (BD Inc.) 24G, 26G and 31G having standard orifice inner-diameter of 0.311 mm, 0.260 mm and 0.133 mm, respectively (Birmingham gauge, [32]). The droplet volumes generated using these needles are 3.1 μl, 2.5 μl and 1.8 μl, respectively with the corresponding standard deviations of 0.17 μl, 0.08 μl and 0.05 μl. An ethanol droplet is generated slowly and allowed to detach from the needle freely under the influence of gravity such that the droplet does not have any initial momentum. The impact height, h (the distance of the tip of the needle from the glass substrate) is varied from 2.4 mm to 6 mm with the help of the syringe clamped in a retort stand. To capture the coalescence dynamics, the side view of the droplet (Figure 1(a)) has been recorded at 2000 frames per second (fps) using a high-speed camera with a long tube objective (Navitar Inc., 12x). A white LED lamp is used to illuminate the background of the droplets. The spatial resolution of the camera is 58 pixels/mm. All experiments were performed in a closed chamber clean room with controlled humidity (45%) and at room temperature (25°C). Thus the crosswind effect is negligible. The density (ρ), viscosity (μ) and surface tension (σ) (with respect to air) of ethanol at 25°C are 789 kg/m^3, 1.095×10^{-3} Pa·s and 0.0221 N/m, respectively. The surrounding medium is air (density of air, ρ_a is 1.225 kg/m^3). Thus, the value of the Atwood number, $At\,(\equiv (\rho - \rho_a)/(\rho + \rho_a))$ is fixed at 0.997 in the present study. The corresponding dimensionless parameters, i.e. the Ohnesorge number (Oh) and the Bond number (Bo) for different sizes of impacting droplet are listed in Table 1.

The following procedure is followed to perform the experiments. First, the syringe with the desired needle size is installed in the retort stand such that the tip of the needle is at a height h from the glass substrate. Then a droplet is released slowly from the needle and is allowed to fall freely under the influence of gravity on the glass substrate. To obtain different sizes of the sessile droplet, we release multiple droplets one after another and wait for some time (2 to 5 seconds) for the resultant sessile droplet to reach a static position on the glass substrate. We use the same needle to create both the sessile droplet and the impacting droplet as it is difficult to change the needle during each experiment. Thus, the volume of the sessile droplet, V_p is an integer multiple of the volume of the impacting droplet. Only in the case of $Vp/Vi = 0.5$, we let evaporate half of the droplet and then release another droplet over it. We verify that when partial coalescence happened, the whole volume of the impacting droplet was integrated into the sessile drop. Evaporation can also be neglected as the time scale for the experiments is only 2-5 seconds, which is much smaller

than the total evaporation time even for the smallest droplet considered (i.e. it takes more than 60 seconds to completely evaporate a droplet of 1.8μL). Strictly speaking, although owing to evaporation the droplet never reaches an equilibrium, the experimental time is so small that a steady contact angle can be assumed. To calculate the droplet volume (V_p) and the contact angle (θ) of the sessile droplet, we analyse and measure the height (h_p) and the wetted diameter (d_p) of the droplet from the side view of the recorded images using "Jasc Paint Shop Pro 7®" image editing software, and the volume of the sessile droplet is calculated using the spherical cap assumption as $V_p = \left[\pi h_p(3(d_p/2)^2 + h_p^2)/6\right]$ and the contact angle as $\theta = \left[2\tan^{-1}(2h_p/d_p)\right]$ [33]. Figure 1(b) shows the variation of the contact angle (θ) of the ethanol droplet with its volume (V_p). It can be seen that the value of θ decreases slightly with the increase in V_p (from $\theta \approx 25^\circ$ at $V_p = 1.8$ μl to $\theta \approx 22.4^\circ$ at $V_p = 9.4$ μl). We release another droplet from the same needle without disturbing the location of the glass substrate and the needle tip. In this way, we ensure that the impacting droplet falls at the apex of the sessile droplet, which is recorded using the high-speed camera. To ensure the repeatability of observed coalescence events, each experiment has been repeated four to five times and the variation in measuring these repeated tests and the highest possible measurement error in each plot is represented by error bar.

3. Results and discussion

The physical parameters involved in the present study are the volume the sessile droplet (V_p), the volume of the impacting droplet (V_i) and the impact height (h)/Weber number (We). We independently vary each parameter by keeping the rest of the parameters fixed and investigate their effect on the coalescence dynamics of the droplets. We have identified the regimes in which the impacting droplet undergoes the partial coalescence and the spreading behaviors in V_p/V_i and We space. In situations involving partial coalescence, the size of the daughter droplet is also obtained as a function of V_p/V_i and We.

3.1. Effect of size of the sessile droplet

To understand the effect of the sessile droplet size on the coalescence dynamics, an impacting spherical droplet of volume, $V_i = 2.5$ μl and an impact height, $h = 2.9$ mm are considered. Here, $Oh = 6.36 \times 10^{-3}$ and $Bo = 1.012$. The volume of the sessile droplet is varied such that $V_p/V_i =$ 0.5, 1, 2 and 3. The temporal evolutions of the coalescence dynamics of the impacting droplet on a sessile droplet for different values of V_p/V_i are presented in Figure 2. The objective of this plot is also to demonstrate the partial coalescence and spreading behaviors of the impacting droplet on the sessile droplet. The instant when the impacting droplet touches the sessile droplet is represented by $t = 0$ for all the results presented in this study. Thus, the time (in ms) written at the top-left corner of each frame in Figure 2 is negative before the droplet touches the sessile droplet and positive after that. The first row in Figure 2 shows the droplets before coalescence ($t < 0$). The red dotted line in each image of this row represents the surface of the substrate below which the symmetrical reflection of the droplet can be seen. The second row in Figure 2 shows the event at which the impacting droplet touches the sessile droplet of different volumes ($t = 0$ ms). The subsequent rows present the coalescence dynamics for different values of V_p/V_i at different times.

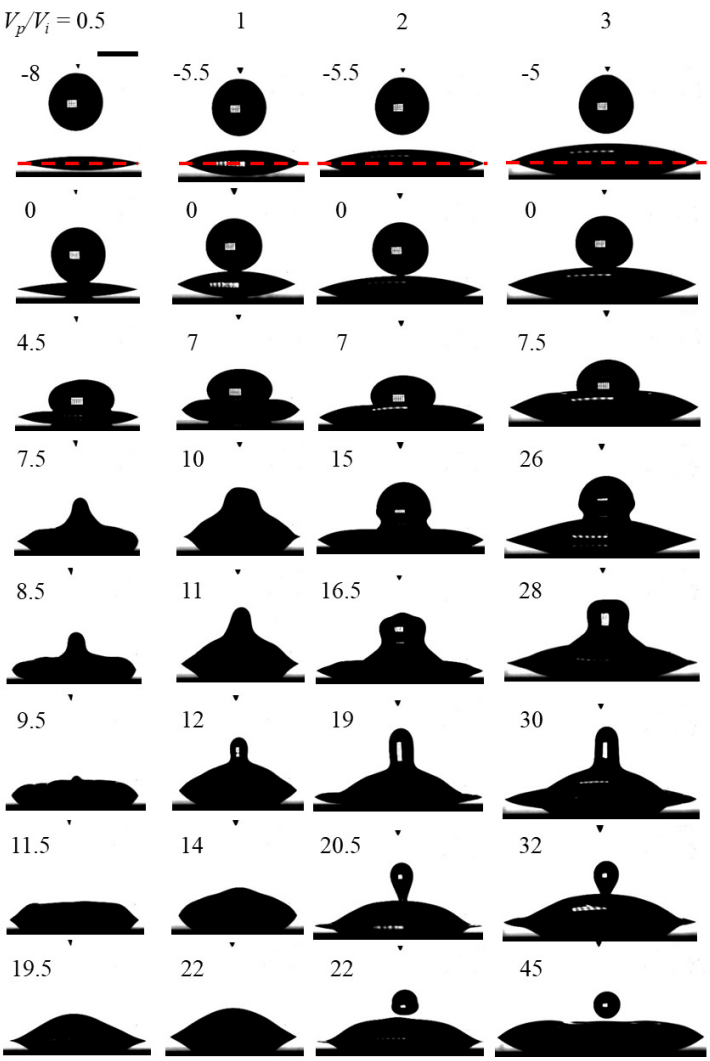

Figure 2: The time evolution of the impacting droplet on a sessile droplet for different values of V_p/V_i for $V_i = 2.5$ μl and $h = 2.9$ mm. Here, $Oh = 6.36 \times 10^{-3}$, $Bo = 1.012$. The black marks at the top of the impacting droplet is the tip of the nozzle. The number in each image represents time, t in ms, which is measured from the instant when the impacting droplet touches the sessile droplet. The red line (shown only for the first row) represents the surface of the substrate and the region below this line is only the reflection. The scale bar shown in the top left panel corresponds to 1 mm. The maximum values of the standard deviation in V_p/V_i and h are 0.06 and 0.1 mm, respectively. Multimedia 1 and 2 demonstrate the coalescence dynamics for $V_p/V_i = 1$ and 2, respectively.

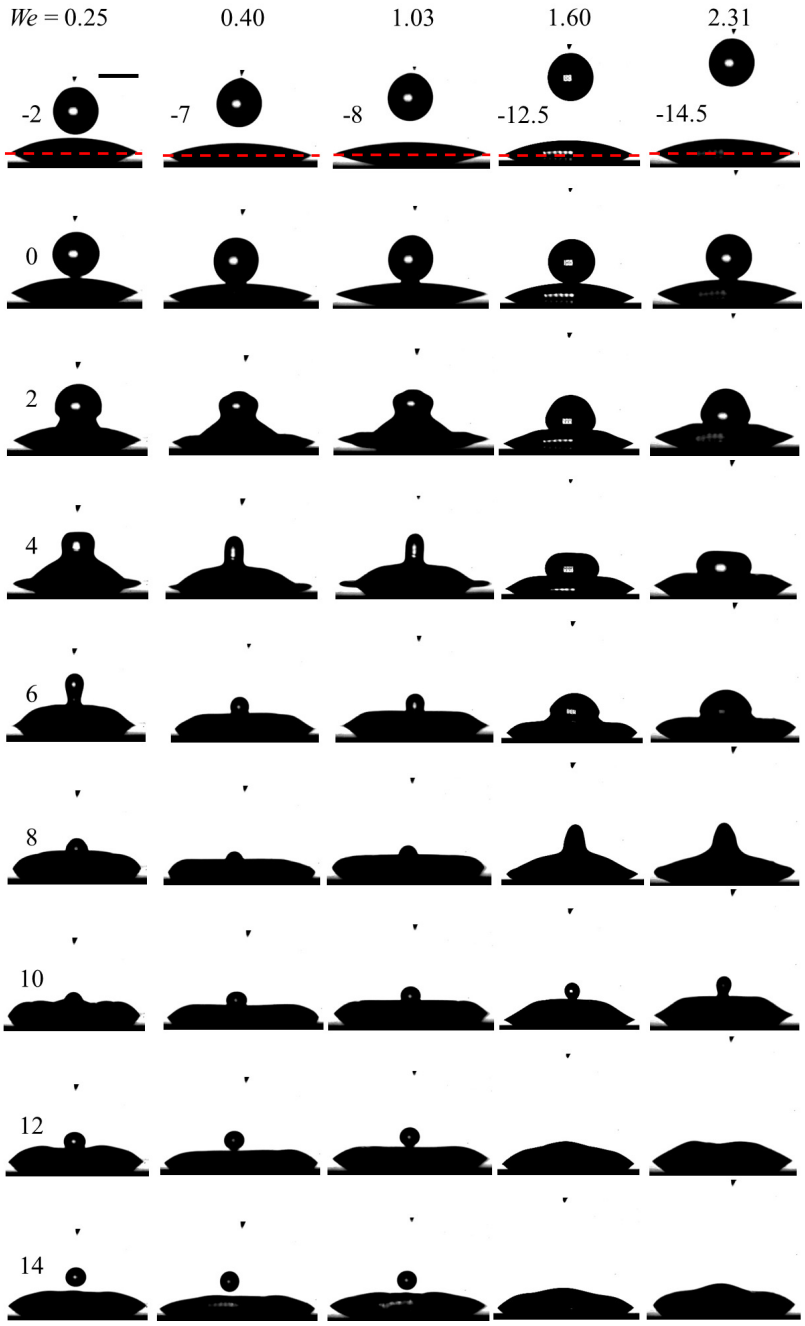

Figure 3: The time evolution of the coalescence dynamics of the impacting droplet on a sessile droplet for different values of Weber number (*We*) for $V_p/V_i = 2$. Here, $Oh = 6.74 \times 10^{-3}$, $Bo = 0.799$. The black marks at the top of the impacting droplet is the tip of the nozzle. The number in each image represents time, t in ms. The red line (shown only for the first row) represents the surface of the substrate. The scale bar shown in the top left panel corresponds to 1 mm. The maximum values of the standard deviation in V_p/V_i and *We* are 0.06 and 0.064, respectively. Multimedia 3 and 4 demonstrate the coalescence dynamics for $We = 2.95$ and 3.72, respectively.

For $V_p/V_i = 0.5$ (first column) and $V_p/V_i = 1$ (second column), the impacting droplet rests on the surface of the sessile droplet for some time (residence time) before it drains and completely coalesces with the sessile droplet without the pinch-off of any daughter droplet (spreading behavior). In these cases, the viscous forces dominate the capillary forces resulting in capillary wave damping resulting in partial coalescence suppression. During this residency period, the air trapped between the droplet and the free surface of the sessile droplet is drained out. It observed that the residence time for $V_p/V_i = 1$ is greater than that of $V_p/V_i = 0.5$. One possible explanation for this behavior could be that as the volume of the sessile drop (V_p) increases, the sessile drop deforms more. As a result, the air layer between the two drops could remain stable for a longer time, which increases the residence time. As we increase the value of V_p/V_i further the coalescence dynamics of the droplet changes from spreading to partial coalescence as the capillary force increases. In case of drop interacting a flat air-liquid interface, this is termed as inertio-capillary regime [8]. It can be seen that for $V_p/V_i = 2$ (third column) and $V_p/V_i = 3$ (fourth column) as the droplet comes in contact with the sessile droplet, after the residence period, the curvature near the contact region becomes sharp (see $t = 7$ ms for $V_p/V_i = 2$; $t = 7.5$ ms for $V_p/V_i = 3$) that generates a large capillary pressure near the contact region. This in turn leads to a rapid expansion of the neck resulting upward-moving capillary waves (see $t = 15$ ms and $t = 16.5$ ms for $V_p/V_i = 2$; $t = 26$ ms and 28 ms for $V_p/V_i = 3$). Thus form a liquid column (see $t = 19$ ms for $V_p/V_i = 2$; $t = 30$ ms for $V_p/V_i = 3$), which is followed by a necking process near the contact region at $t = 20.5$ ms for $V_p/V_i = 2$ and $t = 32$ ms for $V_p/V_i = 3$. As the time progresses, the diameter of the neck of the liquid column reduces due to the inward pull exerted by the surface tension and a daughter droplet pinches off at $t = 22$ ms for $V_p/V_i = 2$ and $t = 45$ ms for $V_p/V_i = 3$. The partial coalescence occurs when the vertical collapse time sufficiently exceeds the horizontal collapse time of the liquid column. Multimedia 1 and 2 demonstrate the coalescence dynamics for $V_p/V_i = 1$ and 2, respectively. The influence of the propagating capillary waves along the interface has been extensively studied by [7, 9, 34–36] for droplet falling in liquid pool. Despite the fact that the capillary waves are stronger in the present case due to their "reflection" from the contact line (see Figures 2 and 3, and Multimedia 1- 4) and the droplet experiences a negative curvature of the sessile droplet in the present configuration. The reflection of capillary wave at the contact line of the droplet can be seen in Figures 2 and 3. The capillary wave is reflected from the contact line region making the droplet thinner at the contact line as it sweeps the liquid mass to the droplet center. We note that the daughter droplet volumes (V_s) are $\approx 0.12V_i$ and $\approx 0.135V_i$ for $V_p/V_i = 2$ and 3, respectively. These are similar to that observed in the case of droplet coalescence in a liquid pool, where $V_s \approx 0.125V_i$. Figure 2 may also conclude that there is a critical value of V_p/V_i (in between 1 to 2) above which the pinch-off or partial coalescence phenomenon happens.

3.2. Effect of impact height or Weber number

Figure 3 shows the effect of the Weber number (*We*) or impact height (h) on the coalescence dynamics of an impacting droplet of size 1.8 μl ($Oh = 6.74 \times 10^{-3}$, $Bo = 0.799$) on a sessile droplet of the critical volume (i.e. $V_p/V_i = 2$). The results are shown in terms of the Weber number ($We \equiv \rho v^2 d_i/\sigma$), where ρ, v, d_i and σ are density, droplet impact velocity just before the onset of coalescence and droplet impact diameter before impact and surface tension, respectively. It can be seen that for low values of *We* (i.e., $We = 0.25$ (first column), $We = 0.40$ (second column)

and $We = 1.03$ (third column)), the impacting droplet undergoes partial coalescence phenomenon, which is qualitatively similar to the ones observed for $V_p/V_i = 2$ and $V_p/V_i = 3$ in Figure 2. As we increase the value of *We* further to $We = 1.60$, a daughter droplet is formed at $t = 10$ but it does not detach from the sessile droplet. This daughter droplet quickly drains into the sessile droplet for $We = 1.60$. On the other hand, for $We = 2.31$, a liquid column is form due to the upward moving capillary waves. In this case, the inertial drainage dominates the capillary force. Thus, the vertical collapse rate is found to be much quicker than the horizontal collapse rate, which suppresses the neck formation and the column drains into the sessile droplet (spreading dynamics). Hence, there is critical value of *We* below which the partial coalescence occurs. In this case, the critical value of *We* is 1.03. Close inspection of Figure 3 also reveals that the residence period decreases with increase in the value of *We*. Multimedia 3 and 4 demonstrate the coalescence dynamics for $We = 1.03$ and 1.60, respectively.

3.3. Regime map

As the coalescence dynamics of the droplet depends on both V_p/V_i and *We*, we plot the regime maps identifying the partial coalescence (solid symbols) and the spreading (open symbols) behaviours in the V_p/V_i - *We* space for different sizes of the impacting droplet, namely, $V_i = 1.8\ \mu$l ($Oh = 6.74\times10^{-3}$, $Bo = 0.799$), $2.5\ \mu$l ($Oh = 6.36\times10^{-3}$, $Bo = 1.012$) and $3.1\ \mu$l ($Oh = 6.16\times10^{-3}$, $Bo = 1.147$) in Figures 4(a), (b) and (c), respectively. It is interesting to note that for all sizes of the impacting droplet considered, the critical value of V_p/V_i above which partial coalescence occurs for small values of *We* is found to be 2, below which the impacting droplet coalesces completely without any pinch-off or daughter droplet generation. Of course, it is to be noted that due to the experimental limitations, we could not perform experiments for V_p/V_i between 1 and 2. The critical Weber number (*We*) above which the droplet exhibits spreading phenomenon increases with the increase in the volume of the impacting droplet (V_i). The critical values of *We* for $V_p/V_i \geq 2$ are found to be 1.03, 2.60 and 3.25 for $V_i = 1.8\ \mu$l, $2.5\ \mu$l and $3.1\ \mu$l, respectively. In the case of a droplet falling on another drop resting on a steel nozzle, Zhang et al. [19] also found that the critical value of V_p/V_i is a function of the Ohnesorge number, *Oh*, which is in between 1 and 2 for $Oh \to 0$.

The transition from partial coalescence to full coalescence depends upon the curvature of the sessile and impacting droplet, and competition between vertical collapse rate to horizontal collapse rate. As the Weber number increases, vertical collapse rate increases due to higher kinetic energy of impacting droplet, which suppresses the horizontal collapse rate, hence the neck formation. This results in no-pinch off or full coalescence at a higher value of the *We* and partial coalescence at lower *We*. On the other hand, in the case of larger droplets ($V_p/V_i \geq 2$), the capillary forces start to dominate over the viscous forces and hence results in pinch-off of a daughter droplet.

3.4. Size of daughter droplet

Next we investigate the size of the daughter droplet above the critical value of V_p/V_i and below the critical value of *We* (i.e in the region of partial coalescence) for different values of V_i. In Figures 5(a) and (b), we present the variations of V_s/V_i versus V_p/V_i for $We = 1.01 \pm 0.05$ and V_s/V_i versus *We* for $V_p/V_i = 2 \pm 0.06$, respectively for three values of V_i (i.e. $V_i = 3.1\ \mu$l, $2.5\ \mu$l and $1.8\ \mu$l). The error bars associated with the measurement of V_s/V_i, V_p/V_i and *We* are 0.027, 0.06 and

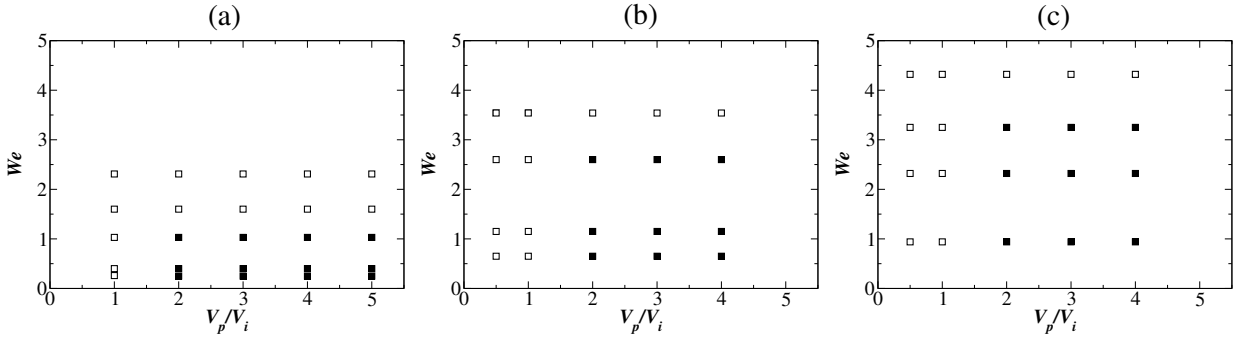

Figure 4: Regime maps showing the partial coalescence (solid symbols) and the spreading (open symbols) behaviours in V_p/V_i and *We* space for different sizes of the impacting droplet: (a) V_i = 1.8 μl (b) V_i = 2.5 μl and (c) V_i = 3.1 μl. The maximum values of the standard deviation in V_p/V_i and *We* are 0.06 and 0.076, respectively. In Table 1, the values of *Oh* and *Bo* are listed for different values of V_i.

0.076, respectively. The error bars represent the standard deviation including the measurement error. It can be seen in Figure 5(a) that for the smallest impacting droplet considered (V_i = 1.8 μl), increase in V_p/V_i has an insignificant effect on the normalized size of the daughter droplet (V_s/V_i). In this case, V_s/V_i is approximately constant at 0.13. However, increasing the size of the impacting droplet increases the influence of the size of the sessile droplet on the daughter droplet, i.e. increasing V_p/V_i increases the value of V_s/V_i (size of the daughter droplet) approximately linearly. We observe that for V_i = 2.5 μl, V_s/V_i increases from 0.12 at $V_p/V_i \approx 2$ to 0.152 at $V_p/V_i \approx 4$, and for V_i = 3.1 μl, V_s/V_i increases from 0.1 at $V_p/V_i \approx 2$ to 0.155 at $V_p/V_i \approx 4$. Similarly in Figure 5(b), it can be seen that increasing the Weber number (*We*) increases the value of V_s/V_i for bigger impacting droplets with $V_i \geq 2.5$, but it remains almost constant for the smallest droplet considered (V_i = 1.8 μl). From all the results presented so far, we found that the size of the daughter droplet in the configuration considered in the present study lies in the range of $0.1V_i$ to $0.16V_i$. This is similar to the result observed in case of liquid droplet slowly placed on a horizontal liquid-air interface [8, 9]. Recently, by performing experiments on water droplet impacting a horizontal free water surface at different velocities, Ma et al. [37] showed that the size of the daughter droplet can be even bigger than the primary droplet. Thus the small size of daughter droplets observed in the configuration considered in the present study is attributed to the positive and negative curvature of the impacting and sessile droplets at the time of impact.

Another interesting point to note is that in Figure 3, for *We* = 0.25 - 1.03, the daughter droplets are not from the first generation but are from the second generation as the liquid column (t = 4 − 6 ms) collapses because of drainage (t = 6 − 10 ms) and subsequently the daughter droplet is generated. Zhang et al. [19] studied different generation daughter droplets and found that the size of the second-generation droplets ($d_s/d_i \approx 0.2$) are usually smaller than the first generation drops ($d_s/d_i \approx 0.5$). Also, some drops (as shown in Figure 2) are the first generation daughter droplets. This explains the two levels of V_s/V_i observed in Figure 5(b).

3.5. Pinch-off time of daughter droplet

Finally, Figures 6(a) and (b) show the effect of varying V_p/V_i and *We* on the pinch-off time of the daughter droplet, t_s (i.e. the value of t at which the daughter droplet pinches off) normalised

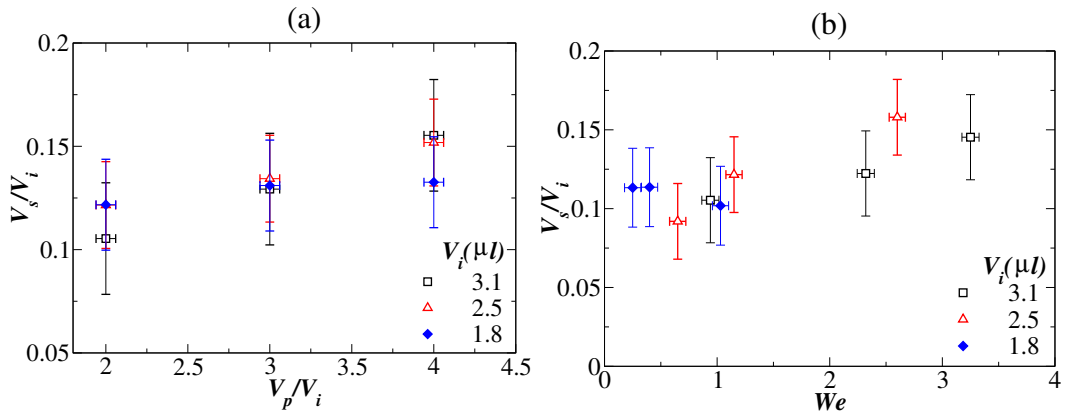

Figure 5: Variations of the normalised volume of the daughter droplet (V_s/V_i) with (a) the normalised volume of the sessile droplet (V_p/V_i) and (b) the Weber number (We) for different values of the volume of the impacting droplet (V_i). The lengths of error bars in V_s/V_i, V_p/V_i and We are 0.027, 0.06 and 0.076, respectively. In Table 1, the values of Oh and Bo are listed for different values of V_i.

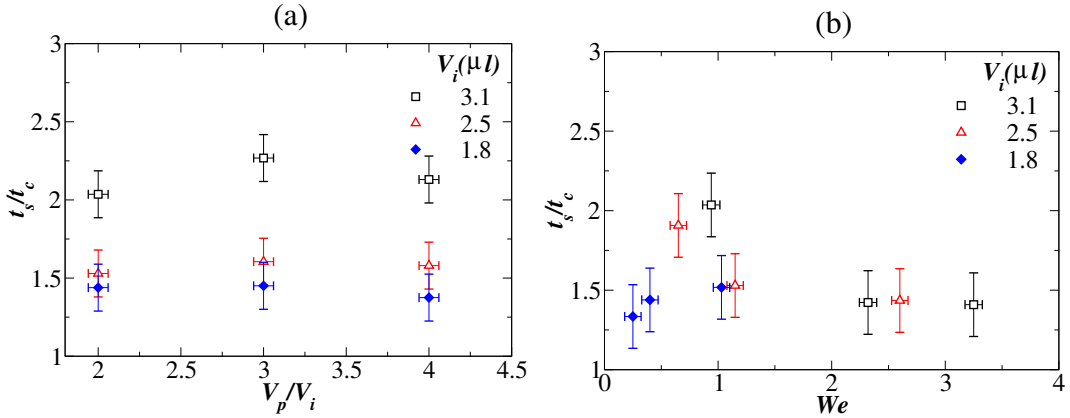

Figure 6: Variations of the normalised pinch-off time with the capillary time scale ($t_c \equiv \sqrt{\rho d_i^3/\sigma}$) versus (a) the normalised volume of the sessile droplet (V_p/V_i) and (b) the Weber number (We) for different values of the volume of the impacting droplet (V_i). The lengths of error bars in t_s/t_c, V_p/V_i and We are 0.2, 0.06 and 0.076, respectively. In Table 1, the values of Oh and Bo are listed for different values of V_i.

with the capillary time scale, $t_c \equiv \sqrt{\rho d_i^3/\sigma}$. The capillary time scale is obtained by balancing the inertial and the surface tension forces. Figure 6(a) shows the variations of t_s/t_c with V_p/V_i for different values of V_i at $We = 1.01 \pm 0.05$. It can be seen that t_s/t_c remains almost constant for each volume of the impacting droplet (V_i). However, for a fixed value of V_p/V_i, t_s/t_c increases with the increase in V_i. Effect of the Weber number (We) on t_s/t_c is shown in figure 6(b) for different values of V_i for a fixed value of $V_p/V_i = 2 \pm 0.06$. It can be seen that t_s/t_c decreases with the increase in We and reaches to plateau at around 1.4 for $V_i \geq 2.5$ μl. For small impacting droplet ($V_i = 1.8$ μl), t_s/t_c is almost constant ($t_s/t_c \approx 1.4$). This behaviour can also be observed qualitatively in Figure 3, where the temporal evolution of the coalescence dynamics for different values of We is presented.

4. Concluding remarks

The coalescence dynamics of ethanol droplet falling on a sessile ethanol droplet has been investigated experimentally. The phenomena reported in the present study are applicable for $6.16 \times 10^{-3} \leq Oh \leq 6.74 \times 10^{-3}$, $0.799 \leq Bo \leq 1.147$ and $0.25 \leq We \leq 4.32$. The effects of the sessile droplet volume (V_p), impacting droplet volume (V_i) and impact height (h) or the Weber number(We) on the coalescence dynamics are studied. The regime maps showing the partial coalescence and spreading behaviors of the impacting droplet are presented in V_p/V_i - We space for different sizes of the impacting droplet. It is found that the partial coalescence phenomenon occurs for $V_p/V_i \geq 2$ and $We \leq 1.03$, 2.60 and 3.25 for $V_i = 1.8$, 2.5 and 3.1 μl, respectively. The normalised size of the daughter droplet (V_s/V_i) increases with the increase in the normalised size of the sessile droplet (V_p/V_i) and the Weber number (We). The values of V_s/V_i for all the parameters considered are found to lie in the range of 0.09 - 0.16. This is very similar with the coalescence dynamics observed for droplets slowly placed on a horizontal liquid-air interface in the inertio-capillary regime, where the value of $V_s/V_i \approx 0.125$ [8]. The positive and negative curvatures of the impacting and the sessile droplet at the time of impact and the reflected capillary waves from the contact line are found to play a significant role in the present configuration. The pinch-off time normalised with the capillary time scale does not vary significantly with V_p/V_i, but increases with increasing the size of the impacting droplet. Increasing We for a fixed value of V_p/V_i decreases the value of the normalised pinch-off time, which reaches a plateau for high values of We. As the contact angle of the sessile drop is expected to influence the coalescence phenomenon, it is interesting to explore the effect of the nature of the substrate in the future.

[1] J. J. Thomson, H. F. Newall, On the formation of vortex rings by drops falling into liquids, and some allied phenomena, Proc. Royal Soc. Lond. 39 (239-241) (1886) 417–436.

[2] A. M. Worthington, A study of splashes, Longmans, Green, and Co, 1908.

[3] H. A. Stone, A. D. Stroock, A. Ajdari, Engineering flows in small devices: microfluidics toward a lab-on-a-chip, Annu. Rev. Fluid Mech. 36 (2004) 381–411.

[4] C. Josserand, S. T. Thoroddsen, Drop impact on a solid surface, Ann. Rev. Fluid Mech. 48 (2016) 365–391.

[5] S. Wildeman, C. W. Visser, C. Sun, D. Lohse, On the spreading of impacting drops, J. Fluid Mech. 805 (2016) 636–655.

[6] H. Deka, G. Biswas, S. Chakraborty, A. Dalal, Coalescence dynamics of unequal sized drops, Phys. Fluids 31 (1) (2019) 012105.

[7] F. Blanchette, T. P. Bigioni, Partial coalescence of drops at liquid interfaces, Nat. Phys. 2 (5) (2006) 254–257.

[8] X. Chen, S. Mandre, J. J. Feng, Partial coalescence between a drop and a liquid-liquid interface, Phys. Fluids 18 (5) (2006) 051705.

[9] B. Ray, G. Biswas, A. Sharma, Generation of secondary droplets in coalescence of a drop at a liquid-liquid interface, J. Fluid Mech. 655 (2010) 72–104.
[10] G. E. Charles, S. G. Mason, The mechanism of partial coalescence of liquid drops at liquid/liquid interfaces, J. Colloid Sci. 15 (2) (1960) 105–122.
[11] S. T. Thoroddsen, K. Takehara, The coalescence cascade of a drop, Phys. Fluids 12 (2000) 1265–1267.
[12] D. Morton, M. Rudman, L. Jong-Leng, An investigation of the flow regimes resulting from splashing drops, Phys. Fluids 12 (2000) 747–763.
[13] X. Chen, S. Mandre, J. J. Feng, An experimental study of the coalescence between a drop and an interface in Newtonian and polymeric liquids, Phys. Fluids 18 (2006) 092103.
[14] B. Ray, G. Biswas, A. Sharma, Regimes during liquid drop impact on a liquid pool, J. Fluid Mech. 768 (2015) 492–523.
[15] F. H. Zhang, M.-J. Thoraval, S. T. Thoroddsen, P. Taborek, Partial coalescence from bubbles to drops, J. Fluid Mech. 782 (2015) 209–239.
[16] X. Cheng, Y. Zhu, L. Zhang, D. Zhang, T. Ku, Numerical analysis of deposition frequency for successive droplets coalescence dynamics, Phys. Fluids 30 (4) (2018) 042102.
[17] H. Deka, G. Biswas, K. C. Sahu, Y. Kulkarni, A. Dalal, Coalescence dynamics of a compound drop on a deep liquid pool, J. Fluid Mech. 866 (2019) R2 1–11.
[18] X. Tang, A. Saha, C. K. Law, C. Sun, Bouncing-to-merging transition in drop impact on liquid film: Role of liquid viscosity, Langmuir 34 (8) (2018) 2654–2662.
[19] F. H. Zhang, E. Q. Li, S. T. Thoroddsen, Satellite formation during coalescence of unequal size drops, Phys. Rev. Lett. 102 (2009) 104502.
[20] P. J. Graham, M. M. Farhangi, A. Dolatabadi, Dynamics of droplet coalescence in response to increasing hydrophobicity, Phys. Fluids 24 (11) (2012) 112105.
[21] J. Qian, C. K. Law, Regimes of coalescence and separation in droplet collision, J. Fluid Mech. 331 (1997) 59–80.
[22] C.-K. Kuan, K.-L. Pan, W. Shyy, Study on high-Weber-number droplet collision by a parallel, adaptive interface-tracking method, J. Fluid Mech. 759 (2014) 104–133.
[23] S. Farokhirad, J. F. Morris, T. Lee, Coalescence-induced jumping of droplet: Inertia and viscosity effects, Phys. Fluids 27 (10) (2015) 102102.
[24] M. Liu, D. Bothe, Numerical study of head-on droplet collisions at high Weber numbers, J. Fluid Mech. 789 (2016) 785–805.
[25] X. Jia, J.-C. Yang, J. Zhang, M.-J. Ni, An experimental investigation on the collision outcomes of binary liquid metal droplets, Int. J. Multiphase Flow 116 (2019) 80–90.
[26] N. Nikolopoulos, G. Strotos, K. S. Nikas, G. Bergeles, The effect of Weber number on the central binary collision outcome between unequal-sized droplets, Int. J. Heat Mass Transf. 55 (7-8) (2012) 2137–2150.
[27] S. Moghtadernejad, M. Tembely, M. Jadidi, N. Esmail, A. Dolatabadi, Shear driven droplet shedding and coalescence on a superhydrophobic surface, Phys. Fluids 27 (3) (2015) 032106.
[28] R. Attarzadeh, A. Dolatabadi, Coalescence-induced jumping of micro-droplets on heterogeneous superhydrophobic surfaces, Phys. Fluids 29 (1) (2017) 012104.
[29] P. M. Somwanshi, K. Muralidhar, S. Khandekar, Coalescence dynamics of sessile and pendant liquid drops placed on a hydrophobic surface, Phys. Fluids 30 (9) (2018) 092103.
[30] N. Nikolopoulos, G. Strotos, K.-S. P. Nikas, M. Gavaises, A. P. Theodorakakos, M. Marengo, G. E. Cossali, Experimental investigation of a single droplet impact onto a sessile drop, Atomization and Sprays 20 (10).
[31] L. K. Malla, R. Bhardwaj, A. Neild, Colloidal deposit of an evaporating sessile droplet on a non-uniformly heated substrate, Colloids Surf. A. 584 (2020) 124009.
[32] S. Yentis, N. P. Hirsch, J. Ip, Anaesthesia and Intensive Care AZ-Print & E-Book: An Encyclopedia of Principles and Practice, 5th Edition, Elsevier Health Sciences, New York, 2013.
[33] P.-G. De Gennes, Wetting: statics and dynamics, Rev. Mod. Phys 57 (3) (1985) 827.
[34] S. T. Thoroddsen, B. Qian, T. G. Etoh, K. Takehara, The initial coalescence of miscible drops, Phys. Fluids 19 (7) (2007) 072110.
[35] H. Ding, E. Q. Li, F. H. Zhang, Y. Sui, P. D. M. Spelt, S. T. Thoroddsen, Propagation of capillary waves and ejection of small droplets in rapid droplet spreading, J. Fluid Mech. 697 (2012) 92–114.

[36] H. Deka, B. Ray, G. Biswas, A. Dalal, P.-H. Tsai, A.-B. Wang, The regime of large bubble entrapment during a single drop impact on a liquid pool, Phys. Fluids 29 (9) (2017) 092101.
[37] H. Ma, C. Liu, X. Li, H. Huang, J. Dong, Deformation characteristics and energy conversion during droplet impact on a water surface, Phys. Fluids 31 (6) (2019) 062108.